COMPDYN 2025
10th ECCOMAS Thematic Conference on
Computational Methods in Structural Dynamics and Earthquake Engineering
M. Papadrakakis, M. Fragiadakis (eds.)
Rhodes Island, Greece, 15-18 June 2025

CODE-BASED SEISMIC SAFETY-CHECKING OF HISTORICAL MASONRY BUILDINGS

Daniel Caicedo[1], **Shaghayegh Karimzadeh**[1], **Vasco Bernardo**[1], **and Paulo B. Lourenço**[1]

[1] University of Minho
Department of Civil Engineering, ISISE, Campus de Azurém 4800-058
Guimarães, Portugal.
{ dcaicedod, shaghkn, vbernardo, pbl }@civil.uminho.pt

Abstract

This investigation compares the guidelines for seismic safety-checking with limited number of records provided in the current and upcoming versions of Eurocode 8 (EN 1998-1:2005 and prEN 1998-1:2023) for the case of historical masonry buildings. A case study representative of stiff monumental buildings is modelled in OpenSees using 3D macroelements to account for in-plane (IP) and out-of-plane (OOP) effects. Ten suites of motions are defined according to the version of the code, the seismological constraints accounted for in the preselection process, the range of matching in the period domain, and the matching strategy, either uniform scaling or spectral matching. Additionally, selection is performed in soil profiles B and C to examine the effect of soil amplification. Non-linear time-history analyses are conducted, and the distribution of numerical data is analysed for each set. Based on the numerical findings of this research, some important observations regarding the consideration of seismological constraints, matching range, and the minimum number of records, are provided for the selection and scaling of earthquake motions for seismic evaluation of historical masonry buildings.

Keywords: Historical masonry buildings; Eurocode 8; Ground motion selection and scaling; Spectral matching; Non-linear analysis; Out-of-plane response.

1 INTRODUCTION

The selection and scaling of seismic inputs is recognised as a main source of bias and uncertainty in the assessment of engineering structures through non-linear dynamic analyses [1]. State-of-Art reviews concerning the principal methodologies for the selection of 'appropriate' sets of records for earthquake assessment of structural systems were conducted by Katsanos et al. [2], and more recently by Caicedo et al. [1]. Both of them examined different strategies for the selection and scaling of real records to match a target spectrum defined by code provisions or alternative targets such as the uniform hazard spectrum (UHS) [3,4] and the conditional mean spectrum (CMS) [5,6]; intensity measure (IM) based selection for probabilistic assessment [7–12]; and the utilisation of artificial signals as an alternative to ground motion selection and scaling [13–18]. Either because of large complexity or excessive time consumption, in the case of probabilistic approaches, almost none of the above-mentioned techniques are common in conventional engineering practice. To tackle this limitation, seismic codes, such as Eurocode 8 [19], American Standards ASCE/ SEI 41-13 [20] and ASCE/SEI 7-10 [21], or the New Zealand Standard NZS 1170.5:2004 [22], provided simplified guidelines for selection and scaling of input motions. Yet, there are not many investigations available in the literature addressing seismic safety-checking through code-compliant sets of records.

Sextos et al. [23] quantified the impact of the Eurocode 8's approach on the structural performance of an irregular Reinforced Concrete (RC) building damaged during the Lefkada 2003 earthquake in Greece. Koboevic et al. [24] studied the influence of selection and scaling matching the 2005 National Building Code of Canada (NBCC 2005) [25] UHS on the median inelastic brace deformations of a four-story concentrically braced steel frame. Michaud and Léger [26] tested the effectiveness of seven scaling methods and two spectral matching approaches with the NBCC 2005 UHS considering historical and simulated records. Later, Ergun and Ates [27] highlighted the large variability with respect to scaled sets of far-field and near-field ground motions following the criteria for time domain scaling provided in ASCE 7-05 and Eurocode 8. Araújo et al. [28] compared code-based selection methods [19–22] with emphasis on the number of records required for the estimation of the mean seismic response. Karimzadeh et al. [29] studied the effects of ASCE/ SEI 7-16 and Eurocode 8 selection criteria on estimating the seismic demand of an unreinforced masonry shear wall. Jalayer et al. [30] pointed out that the average code-based safety-checking could end up being unconservative with respect to performance-based procedures because of epistemic uncertainties referred to the record-to-record variability (i.e., when the number of records is small). More recently, Vuoto et al. [31] generated geometrical models of architectural heritage, exemplified by the Temple of Vesta in Tivoli, and adopted code-based selection criteria to study the impact of local failure mechanisms through nonlinear dynamic analyses.

This paper explores the seismic safety-checking of historical masonry buildings subjected to bi-directional loading while comparing the code-based guidelines for earthquake selection and scaling delivered in current and upcoming versions of Eurocode 8 [32]. The case study building corresponds to a two-storey stiff monumental heritage structure modelled in OpenSees [33] to account for in-plane (IP) and out-of-plane (OOP) failure mechanisms through three-dimensional macroelements [34]. The effects of non-linear floor-to-wall connections and wall-to-wall interlocking are also considered in the models [35]. Ten sets of accelerograms are defined by alternating the Eurocode 8 version, seismological constraints, range of matching, and matching strategy (i.e., uniform scaling, US; or spectral matching, SM). Two alternative soil classes, namely B and C according to Eurocode 8 [32] soil classification, are investigated. The non-linear response obtained through time-history analyses is thoroughly investigated in terms of mean and dispersion for each set and soil class. Some important remarks are drawn concerning

the ground motion selection and scaling oriented to the safety-checking of historical masonry buildings.

2 CASE STUDY DEFINITION AND NUMERICAL MODELLING

2.1 Building description

The Holsteiner Hof building is a 2-storey stone masonry building representative of stiff monumental heritage structures. The building has a regular rectangular plan with dimensions of 26.00 m × 14.00 m. The height of each storey is 4.50 m. Wall and spandrels thicknesses are 60 cm and 30 cm, respectively. Triangular gables at the top have a thickness of 45 cm. The floor system is composed of timber beams, simply supported on the walls in the shorter direction, and a layer of planks nailed directly to the beams. Hence, horizontal forces are assumed to be transferred as friction forces. The roof system is composed of a wooden truss structure. Minor retrofitting interventions were reported during 1976–1979 that, in general, did not modify the structural system.

2.2 Modelling approach

The three-dimensional macroelement formulation introduced by Vanin et al. [34] for modelling the IP and OOP response of masonry walls is adopted for the large-scale representation of the building. The macroelement is available in the OpenSees library [33] and it is formulated as a one-dimensional element with two nodes at the element ends and one additional node at the midspan. The macroelement is able to capture the IP and OOP response through three sectional models applied at the element ends and at the central section which can reproduce deformation across the main axes. Furthermore, P-Δ formulation is considered to capture the nonlinear geometrical effects. Considering the rotations and lumped shear deformations at the central node, drift values can be calculated individually for flexural and shear deformations. Exceeding the limits in drift values will lead to the loss of lateral strength of the element.

Deformable timber floors cannot be idealised as rigid diaphragms. Thus, the floor system is modelled using orthotropic elastic membranes with higher stiffness in the direction of the beam span, and a lower stiffness in the other direction. The membrane definition is given by the two moduli of elasticity in the orthogonal directions, shear modulus, and thickness of the diaphragm. Although the floors are assumed to be linear elastic, the floor-to-wall connections are modelled to account for nonlinear behaviour and potential connection failure at the beam support that can result in the OOP failure of a pier element. Zero-length elements are used to model the frictional interfaces and possible relative displacement between the nodes. Sliding is allowed in the perpendicular direction to the wall while pounding in the opposite direction. Finally, a zero-length wall-to-wall interface with linear elastic behaviour in compression, no crushing, and a finite tensile strength with exponential softening is used to simulate the formation of vertical cracks and separation of the orthogonal walls due to poor interlocking, which might lead to potential OOP failure of the macroelement.

Table 1 summarises the modelling parameters assumed as the mean or median values reported by [36]. Additional modelling parameters such as the pre-peak deformability in shear (G_c), drift at 20% force capacity loss, and residual friction coefficient (μ_R) are defined after literature survey [37–40].

Table 1. Masonry and modelling parameters.

Parameter	Unit	Definition	Mean value
		Masonry Parameters	
E_m	[Pa]	Modulus of elasticity [37–39]	3.5 × 109

G_m	[Pa]	Shear modulus [37–39]	1.5 × 109*
f'_{cm}	[Pa]	Compressive strength [37–39]	1.3 × 106
c_m	[Pa]	Cohesion [37–39]	2.33 × 105*
μ_m	[-]	Friction coefficient [37–39]	0.25*
P	[kg]	Density [37–39]	2000
		Modelling Parameters	
k_{floor}	[-]	Floor stiffness factor [41,42]	1*
f_w	[-]	Wall-to-wall connection factor [43]	1*
$\mu_{f\text{-}w}$	[-]	Floor-to-wall friction coefficient [44]	1*
$\delta_{c,flexure}$	[-]	Drift capacity in flexure [45]	0.01035*
$\delta_{c,shear}$	[-]	Drift capacity in Shear [45]	0.007*
ζ	[-]	Damping ratio [35]	0.05

Note: (*) symbol over the values, denotes median value taken from a lognormal distribution.

For the non-linear dynamic simulations, a 5% proportional Rayleigh damping is assumed. A secant stiffness damping model is adopted to avoid overdamping in the OOP failure mechanism, and to capture the full OOP rocking response. Figure 1 depicts the Holsteiner Hof building, and numerical modelling developed in OpenSees using 3D macroelements. The vibration periods computed for the first three modes are 0.16 s, 0.14 s, and 0.12 s, respectively.

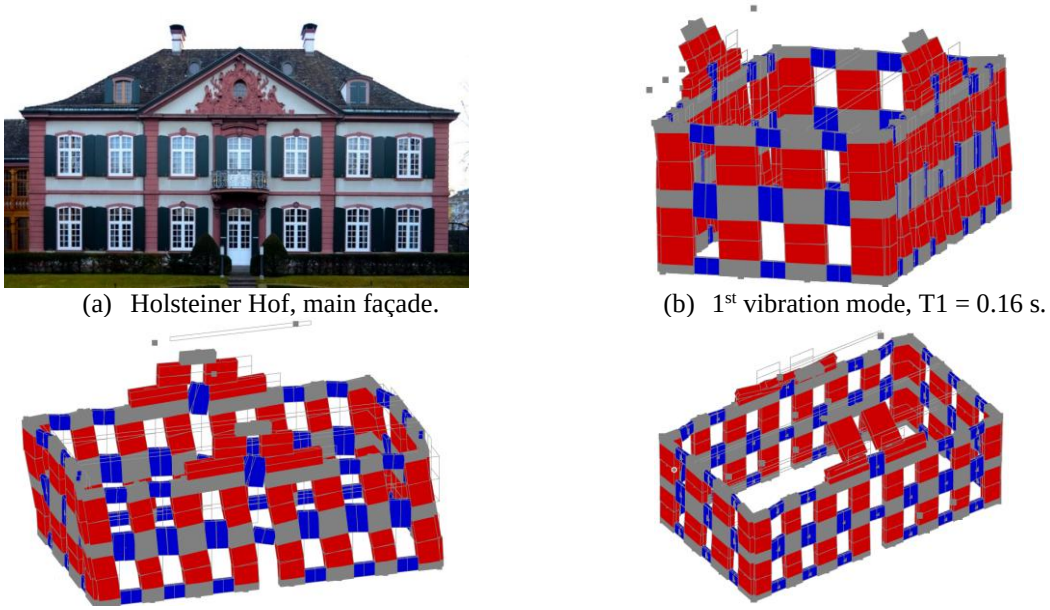

(a) Holsteiner Hof, main façade. (b) 1st vibration mode, T1 = 0.16 s.

(c) 2nd vibration mode, T2 = 0.14 s. (d) 3rd vibration mode, T3 = 0.12 s.

Figure 1. Holsteiner Hof building and numerical model using 3D macroelements.

3 GROUND MOTION SELECTION AND SCALING

3.1 EN 1998-1-1:2004

Current version of the code stablished that the suite of accelerograms for non-linear dynamic analyses should meet the following conditions: (*i*) a minimum of three accelerograms should be used; (*ii*) the mean of the zero-period spectral response acceleration values should not be smaller than the value of a_gS for the site in question; and (*iii*) in the range of periods between $0.2T_1$ and $2T_1$, the mean 5% damped elastic spectrum, calculated from all time histories, should not be less than 90% of the corresponding value of the 5% damped elastic response spectrum. Section 4.3.3.4.3 of the code states that if the response is obtained from at least seven non-linear time-history analyses, the average of the response quantities from all these analyses should be assumed as the structural demand. Otherwise, the most unfavourable value of the response quantity among the analyses should be used. It is also specified that for three-dimensional

analyses, the same accelerogram cannot be used simultaneously along both horizontal directions, and the description of the seismic motion may be made using artificial, recorded or simulated accelerograms.

On the other hand, the elastic response spectrum, S_e, defined in EN 1998-1-1:2004 [19] for the horizontal components of the seismic action is defined by:

$$S_e(T)=\begin{cases} a_g S\left[1+\frac{T}{T_B}(\eta 2.5-1)\right]; if\ 0\le T\le T_B \\ a_g S\eta 2.5\ ;\ if\ T_B\le T\le T_C \\ a_g S\eta 2.5\left[\frac{T_C}{T}\right]\ ;\ if\ T_C\le T\le T_D \\ a_g S\eta 2.5\left[\frac{T_C T_D}{T^2}\right]\ ;\ if\ T_D\le T\le 4s \end{cases} \quad (1)$$

where T is the vibration period of a linear SDOF system; a_g is the design ground acceleration on type A ground, a_{gR}, multiplied by an importance factor γ_I; T_B and T_C are the lower and upper limits of the period in the constant spectral acceleration branch; T_D is the value defining the beginning of the constant displacement response range of the spectrum; S is the soil factor; and η is the damping correction factor with a reference value of $\eta = 1$ for 5% viscous damping. In general, this shape is well-known and easy to reproduce by practitioners in the fields of structural and earthquake engineering.

3.2 prEN 1998-1-1:2023

Annex D provides detailed criteria for selection and scaling of input accelerograms for response-history analyses. The selection should account, as far as possible, for the regional tectonic environment, earthquake magnitude (M_w), source-to-site distance, and local conditions of the recording site, relevant to the return period of the seismic actions of interest. The minimum number of input motions may be reduced to three, for low and very low seismic action classes, considering the most unfavourable peak response; otherwise, a minimum of seven sets of input motions must be used and the average peak response should be considered for estimating the seismic action effects. Simulated and artificial accelerograms are both allowed in the prEN 1998-1-1:2023 edition. Real ones are preferred in regions with available records from qualified strong-motion databases. Subsequently, the following numerical constraints are provided: (*i*) The spectral accelerations of the selected accelerograms should approach the elastic response spectrum in the matching range 0.2 T_1 to 1.5 T_1; (*ii*) The scaling factor should not be larger than 2.0 nor smaller than 0.5; (*iii*) In the matching range $0.2T_1$—$1.5T_1$, the ratio of the average response spectrum to the target response spectrum should fall within the band from 0.75 to 1.3 and should have an average value larger than 0.95; (*iv*) In the matching range $0.2T_1$—$1.5T_1$, the individual spectrum of each accelerogram of the suite should not be out of the ±50% of the target spectrum; (*v*) The suite of motions should not contain simultaneously two components of the same record, and no more than two records from the same earthquake.

In addition to uniform scaling, spectral matching is also allowed. Regarding multi-dimensional analyses, it is specified that compatibility of the horizontal components to the target spectrum should be verified based on the geometric mean of the horizontal spectral accelerations of records, and the orientation of the horizontal components with respect to the principal directions of the structure may be arbitrarily selected. Additionally, in the second-generation of Eurocode 8 the horizontal components of the seismic action are given by:

$$S_e(T)=\begin{cases}\dfrac{S_\alpha}{F_A}\ ;\ if\ 0\le T<T_A\\ \dfrac{S_\alpha}{T_B-T_A}\left[\eta(T-T_A)+\dfrac{T_B-T}{F_A}\right]\ ;\ if\ T_A\le T<T_B\\ \eta S_\alpha\ ;\ if\ T_B\le T<T_C\\ \eta\dfrac{S_\beta T_\beta}{T}\ ;\ if\ T_C\le T<T_D\\ \eta T_D\dfrac{S_\beta T_\beta}{T^2}\ ;\ if\ T\ge T_D\end{cases} \quad (2)$$

$$S_\alpha = F_T F_\alpha S_{\alpha,RP} \quad (3)$$

$$S_\beta = F_T F_\beta S_{\beta,RP} \quad (4)$$

where S_α is the maximum response spectral acceleration (for 5% damping) corresponding to the constant acceleration range of the elastic response spectrum; S_β is the 5%-damped response spectral acceleration at the vibration period T_β = 1s; F_T is the topography amplification factor; T_A is the short-period cut-off associated with the zero-period spectral acceleration; and F_A is the ratio of S_α to the zero-period spectral acceleration. the values of $S_{\alpha,RP}$ and $S_{\beta,RP}$ are taken directly from spectral acceleration maps.

3.3 Sets of records

The derived suites of records depend on the Eurocode version (a and b subindex are assigned to first- and second-generation of Eurocode, respectively) in addition to the seismological constraints, range of matching, and matching strategy. The seismological constraints can be considered as "Fully" or "Relax". When the "Fully" flag is activated, all constraints referred to M_w, R_{JB}, and V_{S30} are accounted for. On the contrary, only M_w and R_{JB} are considered if seismological constraints are set as "Relax". The matching range on the other hand refers to $0.2T_1$–$2T_1$ and $0.2T_1$–$1.5T_1$ for the current and upcoming versions of the Eurocode, respectively. In this sense, the selection depends on the fundamental period of the structure, and it is independent for each building. Additionally, the effect of improving the compatibility with the target spectrum within the entire domain will be also examined. The range of matching is indicated in the column "Domain" as "Range" or "Entire". Lastly, the matching strategy refers to constant-amplitude uniform scaling (US) or spectral matching (SM), for which the academic version of the SeismoMatch v2024 is used. The ten suites of motion are defined in Table 2 and shown in Figure 2 and Figure 3 for soil profiles B and C (i.e., V_{S30} values in the range 360 – 800 and 180 – 360 m/s, respectively). Additional seismological conditions are set as $M_w \ge 4.5$; $R_{JB} \ge 15$ km; and no pulse-like records [46]. The values a_{gR} = 0.15g, $S_{\alpha,RP}$ = 0.35g, and $S_{\beta,RP}$ = 0.10g, needed for deriving the target spectra, were taken from the maps available in the EFEHR Hazard web platform based on the latest European Seismic Hazard Model 2020 (ESHM20) [47] for a site of coordinates (-8.673, 37.102) with moderate to high hazard in accordance with Macedo and Castro [48].

Table 2: Definition of the suites of records for non-linear time-history analyses.

Set	Constraints	Domain	Strategy
1a, 1b	Fully	Range	US
2a, 2b	Relax	Range	US
3a 3b	Fully	Entire	US
4a 4b	Relax	Entire	US
5a 5b	Fully	Entire	SM

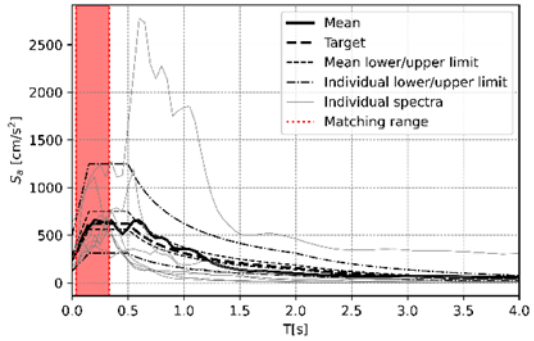

(a) Set 1a

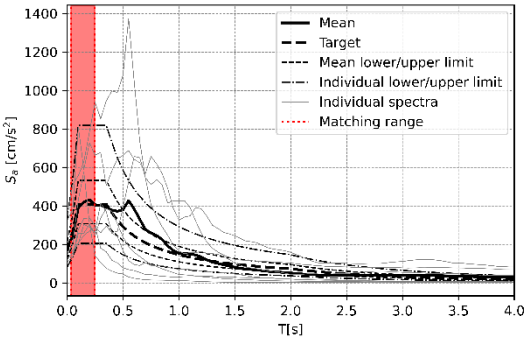

(b) Set 1b

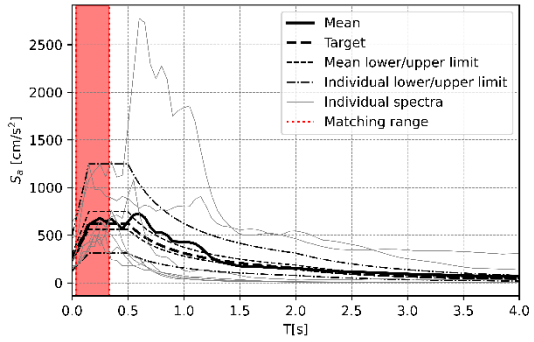

(c) Set 2a

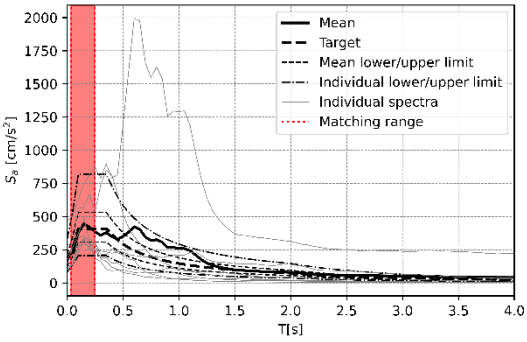

(d) Set 2b

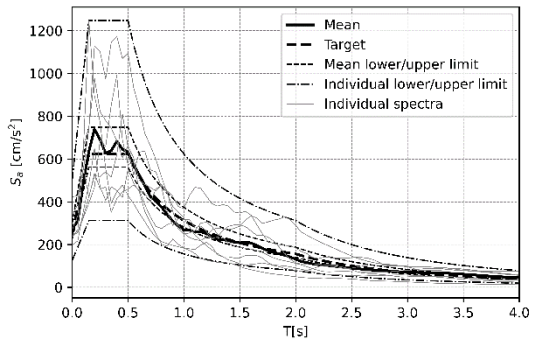

(e) Set 3a

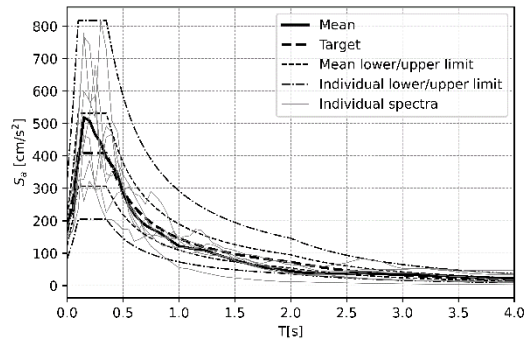

(f) Set 3b

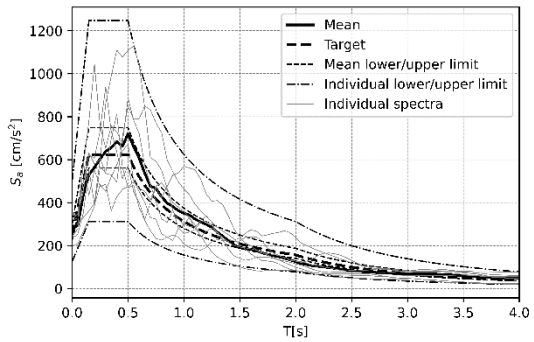

(g) Set 4a

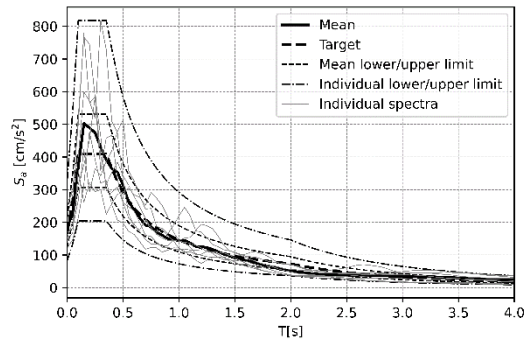

(h) Set 4b

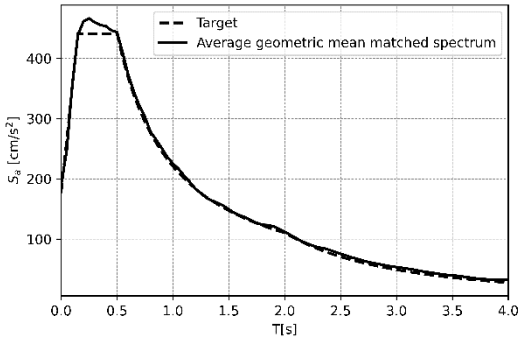

(i) Set 5a

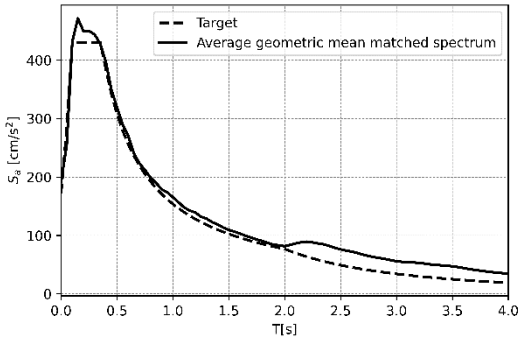

(j) Set 5b

Figure 2: Sets of records — Soil type B.

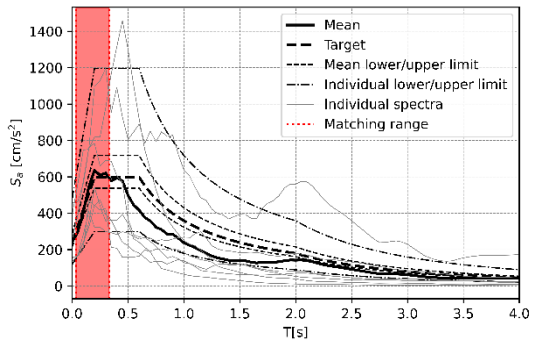

(a) Set 1a

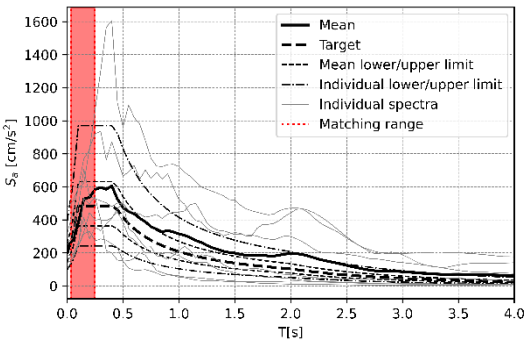

(b) Set 1b

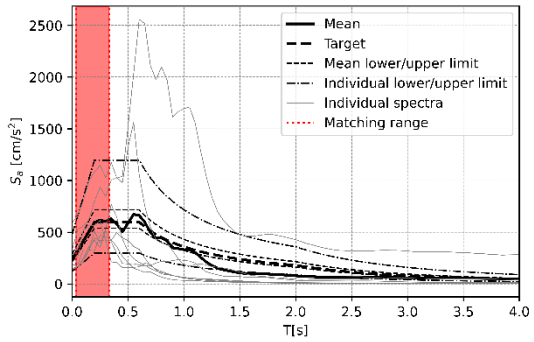

(c) Set 2a

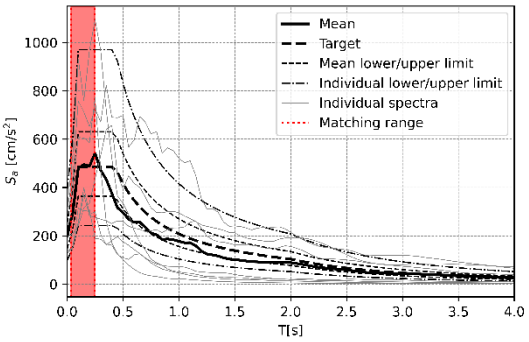

(d) Set 2b

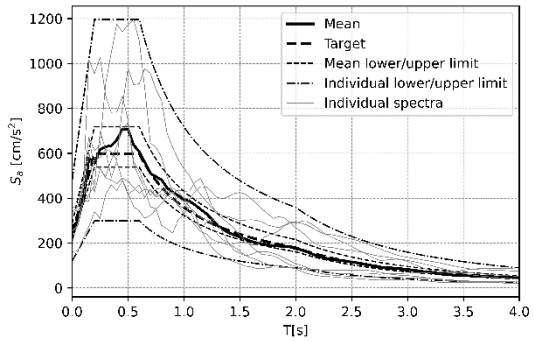

(e) Set 3a

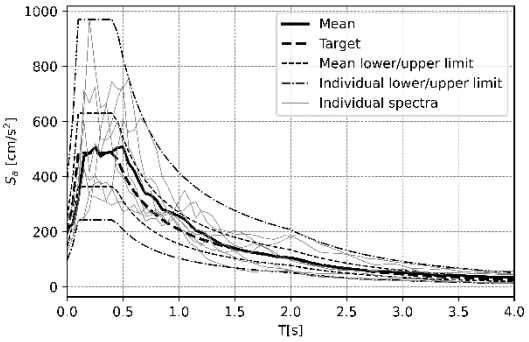

(f) Set 3b

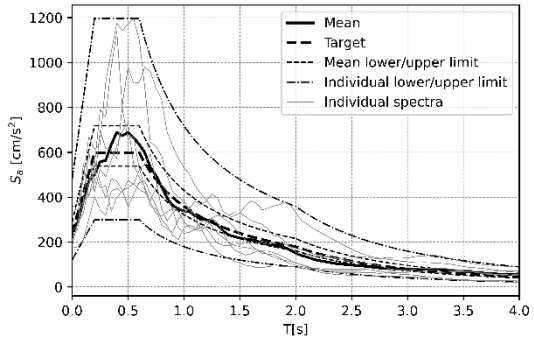

(g) Set 4a

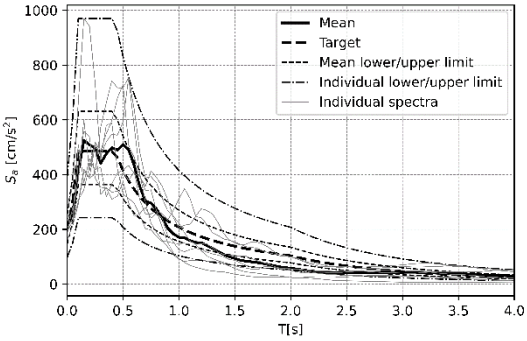

(h) Set 4b

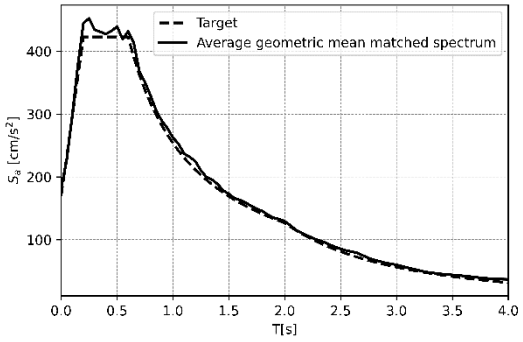

(i) Set 5a

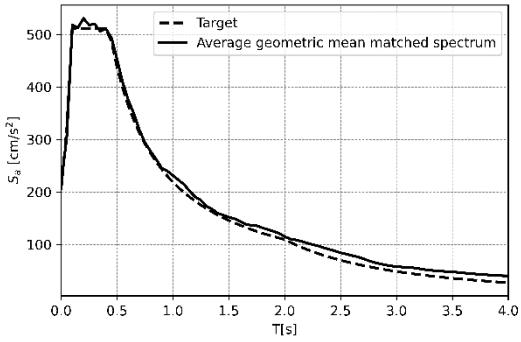

(j) Set 5b

Figure 3: Sets of records — Soil type C.

4 ANALYSIS OF RESULTS

Figure 4 and Figure 5 show the numerical results in terms of max($\overline{\Delta}_r$) and max(V_b), for soil types B and C, respectively. Box-whisker diagrams are employed show the distribution of numerical data for each set of ground motion records. The shape of the box provides a clean representation of the general trend of the data emphasising the median values of each ground motion set. The whiskers (the lines extending from the box on both sides) extend to the minimum and maximum data values of EDP. Outliers are identified as the values that fall above or below the end of the whisker. Additionally, collapse and non-collapse observations are depicted independently within the plots to show a more consistent statistical representation of the data (collapse is identified with a multiplier of records numbers, in case more than one collapse is found). As in [49], asymptotic values of 40.00 mm and 4000 kN are set to denote the global collapse in terms of max($\overline{\Delta}_r$) and max(V_b) metrics. For soil type B, the median of the max($\overline{\Delta}_r$) ranges between 2.84 mm for set 2b and 11.54 mm for set 4a (See Figure 4a); while the median of max(V_b) in Figure 4b oscillates between 1640 kN and 2400 kN, in reference to the same sets, 2b and 4a, respectively. Further, sets 1b and 2b (i.e., US with full and partial consideration of seismological constraints targeting the new shape of the soil B spectrum) lead to the highest dispersion in terms of max($\overline{\Delta}_r$) and max(V_b). The maximum non-collapse observations are made in sets 4a and 3a, and they correspond to max($\overline{\Delta}_r$) = 34.62 mm, and max(V_b) = 3763 kN. Likewise, the minimum values are max($\overline{\Delta}_r$) = 1.97 mm, and max(V_b) = 1325 kN, both observed in set 1a. In opposition, the lowest dispersion for both EDPs is achieved by set 5a (i.e., SM to the old shape of the soil B spectrum) with median values max($\overline{\Delta}_r$) = 7.38 mm, and max(V_b) = 2240 kN.

On the other hand, the amplification in soil shape C leads to more collapse cases, mainly in sets 2a and 1b. The median max($\overline{\Delta}_r$) computed for soil type C varies from 2.64 mm in set 1a up to 13.94 mm for set 4b. Alike, the median value of max(V_b) oscillates between 1660 kN for set 1a and 2750 kN for set 2b. The largest dispersion, or record-to-record variability, is observed within sets 4b and 2b for the max($\overline{\Delta}_r$) and max(V_b), respectively. The peak value of max($\overline{\Delta}_r$) corresponds to 29.63 mm, observed in set 3b, although sets 2b and 3b lead to comparable values. Similarly, max(V_b) = 3565 kN is computed within set 1a. Minimum values of both EDPs are obtained in set 2a corresponding to max($\overline{\Delta}_r$) = 1.80 mm, and max(V_b) = 1345 kN. Set 2a also leads to the lowest record-to-record variability in terms of max($\overline{\Delta}_r$), although that distribution corresponds only to 4 non-collapse observations. Instead, when accounting for all seven records, set 5a provides the smallest dispersion, as in the case of soil type B. In terms of max(V_b), set 5b (i.e., spectral matching to the soil C spectrum shape) shows the lowest dispersion.

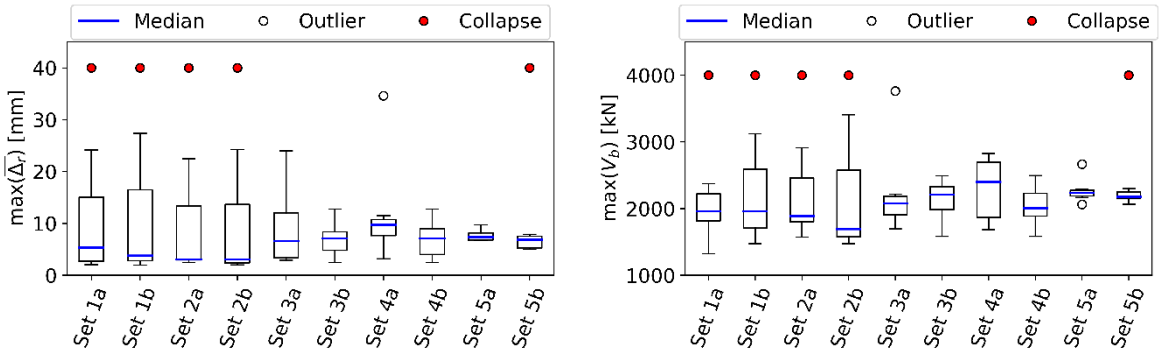

(a) max($\overline{\Delta}_r$) (b) max(V_b)

Figure 4: Box plot — Soil type B.

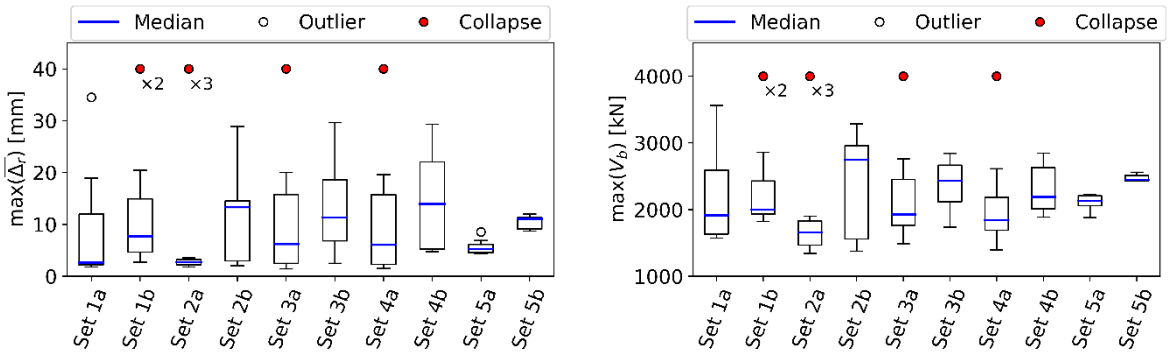

(a) max($\overline{\Delta}_r$) (b) max(V_b)

Figure 5: Box plot — Soil type C.

5 CONCLUSIONS

The code-based safety evaluation of historical masonry buildings subjected to bi-directional horizontal earthquake loads was examined. Numerical model of two-storey stiff historical building was developed in OpenSees accounting for the in-plane (IP) and out-of-plane (OOP) effects of masonry walls, as well as non-linearity in floor-to-wall and wall-to-wall connections. The targets for selection of the input motion were defined based on the spectral shapes provided in the EN 1998-1-1:2004 and prEN 1998-1-1:2023 versions of Eurocode 8 for soil types B and C. Ten sets of motions were defining differing according to the code edition, seismological constraints in the preselection phase, range of matching, and matching strategy (i.e., uniform scaling or spectral matching).

Aimed at reducing the dispersion of the seismic response, the matching strategy should target the full period domain and not just a range defined around the fundamental elastic period, T_1, since higher modes and period lengthening because of cumulative damage play a relevant role in the dynamic behaviour of historical masonry constructions. Similarly, whenever possible, seismological constraints should be accounted for in the preselection process. Spectral matching to the elastic design spectrum defined either in the EN 1998-1-1:2004 and prEN 1998-1-1:2023 versions of Eurocode 8 led to higher estimations of the median response. Alternative less conservative targets are encouraged such as uniform hazard spectrum and conditional mean spectrum. In general, the findings suggest that the minimum number of records that are needed for a reasonable estimation of the *"true"* mean seismic demand should be increased to a value larger than seven. Future work should focus on the application of probabilistic methods on representative masonry archetypes to provide complementary guidance in the process of ground motion selection that is often based only on engineering experience.

ACKNOWLEDGMENT

This study has been partly funded by the STAND4HERITAGE project that has received funding from the European Research Council (ERC) under the European Union's Horizon 2020 research and innovation program (Grant agreement No. 833123), as an Advanced Grant. This work was also partly financed by FCT / MCTES through national funds (PIDDAC) under the R&D Unit Institute for Sustainability and Innovation in Structural Engineering (ISISE), under reference UIDB / 04029/2020 (doi.org/10.54499/UIDB/04029/2020), and under the Associate Laboratory Advanced Production and Intelligent Systems ARISE under reference LA/P/0112/2020. This work is partly financed by national funds through FCT - Foundation for Science and Technology, under grant agreement 2023.01101.BD attributed to the first author.

REFERENCES

[1] Caicedo D, Karimzadeh S, Bernardo V, Lourenço PB. Selection and Scaling Approaches of Earthquake Time-Series for Structural Engineering Applications: A State-of-the-Art Review. Archives of Computational Methods in Engineering 2023. https://doi.org/10.1007/s11831-023-10025-y.

[2] Katsanos EI, Sextos AG, Manolis GD. Selection of earthquake ground motion records: A state-of-the-art review from a structural engineering perspective. Soil Dynamics and Earthquake Engineering 2010;30. https://doi.org/10.1016/j.soildyn.2009.10.005.

[3] McGuire RK. Probabilistic seismic hazard analysis: Early history. Earthq Eng Struct Dyn 2008;37. https://doi.org/10.1002/eqe.765.

[4] Baker JW. An introduction to Probabilistic Seismic Hazard Analysis (PSHA). 2008.

[5] Baker JW, Cornell CA. Spectral shape, epsilon and record selection. Earthq Eng Struct Dyn 2006;35. https://doi.org/10.1002/eqe.571.

[6] Baker JW. Conditional Mean Spectrum: Tool for Ground-Motion Selection. Journal of Structural Engineering 2011;137. https://doi.org/10.1061/(asce)st.1943-541x.0000215.

[7] Huang Y-N, Whittaker AS, Luco N, Hamburger RO. Scaling Earthquake Ground Motions for Performance-Based Assessment of Buildings. Journal of Structural Engineering 2011;137. https://doi.org/10.1061/(asce)st.1943-541x.0000155.

[8] Ay BÖ, Akkar S. Evaluation of a recently proposed record selection and scaling procedure for low-rise to mid-rise reinforced concrete buildings and its use for probabilistic risk assessment studies. Earthq Eng Struct Dyn 2014;43. https://doi.org/10.1002/eqe.2378.

[9] Kazantzi AK, Vamvatsikos D. Intensity measure selection for vulnerability studies of building classes. Earthq Eng Struct Dyn 2015;44. https://doi.org/10.1002/eqe.2603.

[10] Bayati Z, Soltani M. Ground motion selection and scaling for seismic design of RC frames against collapse. Earthquake and Structures 2016;11. https://doi.org/10.12989/eas.2016.11.3.445.

[11] Hariri-Ardebili MA, Saouma VE. Probabilistic seismic demand model and optimal intensity measure for concrete dams. Structural Safety 2016;59:67–85.
[12] Li C, Zhai C, Kunnath S, Ji D. Methodology for selection of the most damaging ground motions for nuclear power plant structures. Soil Dynamics and Earthquake Engineering 2019;116:345–57. https://doi.org/https://doi.org/10.1016/j.soildyn.2018.09.039.
[13] Karimzadeh S, Kadas K, Askan A, Yakut A. Comparison of real and simulated records using ground motion intensity measures. Soil Dynamics and Earthquake Engineering 2021;147. https://doi.org/10.1016/j.soildyn.2021.106796.
[14] Karimzadeh S, Kadasa K, Askanb A, Erberikb MA, Yakutb A. Derivation of analytical fragility curves using SDOF models of masonry structures in Erzincan (Turkey). Earthquake and Structures 2020;18. https://doi.org/10.12989/eas.2020.18.2.249.
[15] Causse M, Laurendeau A, Perrault M, Douglas J, Bonilla LF, Guéguen P. Eurocode 8-compatible synthetic time-series as input to dynamic analysis. Bulletin of Earthquake Engineering 2014;12. https://doi.org/10.1007/s10518-013-9544-2.
[16] Zhong K, Lin T, Deierlein GG, Graves RW, Silva F, Luco N. Tall building performance-based seismic design using SCEC broadband platform site-specific ground motion simulations. Earthq Eng Struct Dyn 2021;50. https://doi.org/10.1002/eqe.3364.
[17] Fayaz J, Dabaghi M, Zareian F. Utilization of Site-Based Simulated Ground Motions for Hazard-Targeted Seismic Demand Estimation: Application for Ordinary Bridges in Southern California. Journal of Bridge Engineering 2020;25. https://doi.org/10.1061/(asce)be.1943-5592.0001634.
[18] Karimzadeh S, Funari MF, Szabó S, Hussaini SMS, Rezaeian S, Lourenço PB. Stochastic simulation of earthquake ground motions for the seismic assessment of monumental masonry structures: Source-based vs site-based approaches. Earthq Eng Struct Dyn 2023. https://doi.org/https://doi.org/10.1002/eqe.4012.
[19] Code P. Eurocode 8: Design of structures for earthquake resistance-part 1: general rules, seismic actions and rules for buildings. Brussels: European Committee for Standardization 2005.
[20] Engineers AS of C. Seismic evaluation and retrofit of existing buildings, American Society of Civil Engineers; 2014.
[21] Engineers AS of C. Minimum design loads and associated criteria for buildings and other structures, American Society of Civil Engineers; 2017.
[22] NZS NZS. Structural design actions Part 5: earthquake actions-New Zealand. Nzs 2004;1170:2004.
[23] Sextos AG, Katsanos EI, Manolis GD. EC8-based earthquake record selection procedure evaluation: Validation study based on observed damage of an irregular R/C building. Soil Dynamics and Earthquake Engineering 2011;31. https://doi.org/10.1016/j.soildyn.2010.10.009.
[24] Koboevic S, Guilini-Charrette K, Castonguay PX, Tremblay R. Selection and scaling of NBCC 2005 compatible simulated ground motions for nonlinear seismic analysis of low-rise steel building structures. Canadian Journal of Civil Engineering 2011;38. https://doi.org/10.1139/L11-094.
[25] NRCC. 2005. National building code of Canada 2005, 12th ed. National Research Council of Canada, Ottawa, Ont. n.d.
[26] Michaud D, Léger P. Ground motions selection and scaling for nonlinear dynamic analysis of structures located in Eastern North America. Canadian Journal of Civil Engineering 2014;41. https://doi.org/10.1139/cjce-2012-0339.
[27] Ergun M, Ates S. Selecting and scaling ground motion time histories according to eurocode 8 and ASCE 7-05. Earthquake and Structures 2013;5. https://doi.org/10.12989/eas.2013.5.2.129.
[28] Araújo M, Macedo L, Marques M, Castro JM. Code-based record selection methods for seismic performance assessment of buildings. Earthq Eng Struct Dyn 2016;45. https://doi.org/10.1002/eqe.2620.
[29] Karimzadeh S, Hussaini SMS, Funari MF, Lourenço PB. On the Effect of Different Code-Based Ground Motion Selection Approaches for the Estimation of the Seismic Demand of Masonry Structures by Using Real Ground Motion Data Set 2021.
[30] Jalayer F, Ebrahimian H, Miano A. Record-to-record variability and code-compatible seismic safety-checking with limited number of records. Bulletin of Earthquake Engineering 2021;19. https://doi.org/10.1007/s10518-020-01024-6.
[31] Vuoto A, Funari MF, Karimzadeh S, Lourenço PB. Generative modelling of Monopteros and Tholos temples using existing data: The case study of Vesta temple in Tivoli. J Cult Herit 2025;71:334–45.
[32] Code P. Eurocode 8: Design of structures for earthquake resistance—Part 3: Assessment and retrofitting of buildings. Incorporating Corrigendum March 2010.
[33] McKenna F. OpenSees: a framework for earthquake engineering simulation. Comput Sci Eng 2011;13:58–66.
[34] Vanin F, Penna A, Beyer K. A three-dimensional macroelement for modelling the in-plane and out-of-plane response of masonry walls. Earthq Eng Struct Dyn 2020;49. https://doi.org/10.1002/eqe.3277.

[35] Vanin F, Penna A, Beyer K. Equivalent-Frame Modeling of Two Shaking Table Tests of Masonry Buildings Accounting for Their Out-Of-Plane Response. Front Built Environ 2020;6. https://doi.org/10.3389/fbuil.2020.00042.
[36] Tomić I, Vanin F, Beyer K. Uncertainties in the seismic assessment of historical masonry buildings. Applied Sciences 2021;11:2280.
[37] Guerrini G, Senaldi I, Scherini S, Morganti S, Magenes G. Material characterization for the shaking-table test of the scaled prototype of a stone masonry building aggregate. Material Characterization for the Shaking-Table Test of the Scaled Prototype of a Stone Masonry Building Aggregate 2017:105–15.
[38] Senaldi I, Guerrini G, Scherini S, Morganti S, Magenes G, Beyer K, et al. Natural stone masonry characterization for the shaking-table test of a scaled building specimen. Proceedings of the International Masonry Society Conferences, vol. 0, 2018.
[39] Guerrini G, Senaldi I, Graziotti F, Magenes G, Beyer K, Penna A. Shake-Table Test of a Strengthened Stone Masonry Building Aggregate with Flexible Diaphragms. International Journal of Architectural Heritage 2019;13. https://doi.org/10.1080/15583058.2019.1635661.
[40] Penna A, Lagomarsino S, Galasco A. A nonlinear macroelement model for the seismic analysis of masonry buildings. Earthq Eng Struct Dyn 2014;43. https://doi.org/10.1002/eqe.2335.
[41] Brignola A, Podestà S, Pampanin S. In-plane stiffness of wooden floor. 2008 NZSEE Conference, Paper 49 2008.
[42] Brignola A, Pampanin S, Podestà S. Experimental evaluation of the in-plane stiffness of timber diaphragms. Earthquake Spectra 2012;28:1687–709.
[43] POLIMI. Critical Review of Methodologies and Tools for Assessment of Failure Mechanisms and Interventions, Deliverable 3.3, Workpackage 3: Damage Based Selection Of Technologies 2010.
[44] Almeida JP, Beyer K, Brunner R, Wenk T. Characterization of mortar–timber and timber–timber cyclic friction in timber floor connections of masonry buildings. Materials and Structures/Materiaux et Constructions 2020;53. https://doi.org/10.1617/s11527-020-01483-y.
[45] Vanin F, Zaganelli D, Penna A, Beyer K. Estimates for the stiffness, strength and drift capacity of stone masonry walls based on 123 quasi-static cyclic tests reported in the literature. Bulletin of Earthquake Engineering 2017;15. https://doi.org/10.1007/s10518-017-0188-5.
[46] Shahi SK, Baker JW. An efficient algorithm to identify strong-velocity pulses in multicomponent ground motions. Bulletin of the Seismological Society of America 2014;104:2456–66.
[47] Danciu L, Nandan S, Reyes C, Basili R, Weatherill G, Beauval C, et al. The 2020 update of the European Seismic Hazard Model: Model Overview. EFEHR Technical Report 001, v1. 0.0 2021.
[48] Macedo L, Castro JM. SelEQ: An advanced ground motion record selection and scaling framework. Advances in Engineering Software 2017;114. https://doi.org/10.1016/j.advengsoft.2017.05.005.
[49] Caicedo D, Tomić I, Karimzadeh S, Bernardo V, Beyer K, Lourenço PB. Optimal intensity measure and probabilistic seismic demand model for the assessment of historical masonry buildings considering in-plane and out-of-plane response. Manuscript Submitted for Publication to Reliability Engineering & System Safety 2024.